Unraveling the activation mechanism of oxidants using copper ferrite nanopowder and its application in the treatment of real waters contaminated by phenolic compounds

Minjuan Cai, Sridhar Gowrisankaran, Maros Gregor, Hryhorii Makarov, Tomas Roch, Jinjun Li, Feng Wu, Gilles Mailhot, Marcello Brigante, Olivier Monfort

Unraveling the activation mechanism of oxidants using copper ferrite nanopowder and its application in the treatment of real waters contaminated by phenolic compounds.

Minjuan Cai[a,b], Sridhar Gowrisankaran[c], Maros Gregor[d], Hryhorii Makarov[d], Tomas Roch[d], Jinjun Li,[b] Feng Wu,[b] Gilles Mailhot,[a] Marcello Brigante[a], Olivier Monfort[c*]

[a]Université Clermont Auvergne, CNRS, Institut de Chimie de Clermont-Ferrand, F-63000 Clermont-Ferrand, France

[b]Department of Environmental Engineering, School of Resources and Environmental Science, Wuhan University, 430079, China

[c]Comenius University Bratislava, Faculty of Natural Sciences, Department of Inorganic Chemistry, Ilkovicova 6, Mlynska Dolina, 842 15 Bratislava, Slovakia

[d]Comenius University Bratislava, Faculty of Mathematics Physics and Informatics, Department of Experimental Physics, Mlynska Dolina, 842 48 Bratislava, Slovakia

*correspondence: (OM) monfort1@uniba.sk; +421290142141

Abstract

Copper ferrites ($CuFe_2O_4$) nanopowder was prepared *via* single pot hydrothermal method followed by annealing at 500°C, and XRD, SEM, XPS and UPS were employed for the material characterization. $CuFe_2O_4$ was employed as the catalyst for the degradation of bisphenol A (BPA) under dark and UVA-illuminated conditions, both in the presence of peroxymonosulfate (PMS) or peroxydisulfate (PDS) as radical precursor under neutral pH values. While the individual processes of photocatalysis (using $CuFe_2O_4$ alone) and photolysis of radical precursors (either PMS or PDS

alone) exhibited limited efficiency in the degradation of BPA, a significant synergistic effect became evident upon combining $CuFe_2O_4$ with PMS or PDS. This led to a notable increase in the degradation constant, with an enhancement of up to 3.8 times under dark and 34 times when PMS was used in the presence of UVA radiation.

Under the most favourable conditions employing 0.5 g L^{-1} of catalyst, the degradation constant of BPA was 0.211 min^{-1} with the use of 2 mM of PMS and 0.018 min^{-1} when 2 mM of PDS were employed. These experiments were conducted under UVA irradiation at pH 6.2, resulting in the complete degradation of BPA within less than 20 min.

The activation mechanism of PMS and PDS using $CuFe_2O_4$ was comprehensively elucidated, revealing sulfate radicals as the primary reactive species in PMS-containing systems, whereas a predominantly non-radical pathway was observed in the presence of PDS. Indeed, XPS indicated that surface copper played an important role in the non-radical pathway. Furthermore, the $CuFe_2O_4$/PMS/UVA and $CuFe_2O_4$\PDS\UVA systems exhibited high performance in efficiently degrading different phenolic compounds including BPA, phenol and p-nitrophenol. These achievements were observed across different real-water matrices with a particular emphasis on sewage treatment plant water.

1. Introduction

Phenolic compounds are well known as persistent and harmful pollutants that are widely present in wastewater from various industries, thus presenting a serious threat to ecosystems and human health [1]. Among these pollutants, bisphenol A (BPA) is an endocrine disrupting compound that can be found in different concentrations in many consumer products such as personal care products,

tableware and medical supplies [2]. Due to its widespread industrial use, BPA has been detected in environmental matrices (such as soil, sediments, groundwater, surface water, air) and food [3]. Other phenolic compounds including phenol and p-nitrophenol which is used in wide variety of organic syntheses and as a pesticide, respectively, can be also bioaccumulated, thus being considered highly toxic [4, 5]. Recently, advanced oxidation processes (AOPs) have attracted a lot of interest for its high efficiency in the treatment of water pollution [6]. Furthermore, compared to the other existing technologies such as adsorption [7], flocculation [8], biodegradation [9] and membrane filtration [10], AOPs are a very promising because they induce rapid degradation of organic pollutants into less harmful substances or completely converting them to carbon dioxide (CO_2), water, and inorganic ions [11]. Usually, hydroxyl radicals ($HO^{\bullet}$, E^0 = 1.9-2.7 V vs. NHE) are the most common reactive oxygen species (ROS) in AOPs and are non-selective for the degradation of almost all organic pollutants. In addition, sulfate radicals ($SO_4^{\bullet-}$) based AOPs (SR-AOPs) have become a more promising research direction since $SO_4^{\bullet-}$ has a longer half-life, greater oxidation capacity (E^0 = 2.5-3.1 V) and a wider pH range stability compared to $HO^{\bullet}$ [12, 13]. Moreover, $SO_4^{\bullet-}$ are more selective for the degradation of organic compounds containing aromatic group constituents than the hydroxyl radicals [14, 15].

Sulfate radicals can be produced by homolytic cleavage of peroxydisulfate (PDS) and unsymmetric cleavage of peroxymonosulfate (PMS), which can be activated by either light, heating, or alkaline earth and transition metals [16-19]. However, these activation processes limit their application at larger scales than laboratory conditions. For example, some transition metal ions are harmful to organisms, thus heterogeneous catalysts being a potential response to these problems. Therefore, the development of transition metal-containing heterogeneous catalysts for the activation

of PDS and PMS for the degradation of organic pollutants has been a popular research topic [20-23].

Many ferrites, including spinel ferrites, have been already reported as efficient catalysts for the degradation of organic pollutants [23, 24]. *M*Fe_2O_4 is the typical formula of spinel ferrites, where *M* = Mn, Ni, Cu, Zn [25-28]. Copper ferrite ($CuFe_2O_4$), has received considerable attention in water treatment due to its high magnetic permeability, excellent chemical and mechanical stability and has been extensively used in PDS and PMS activation [29-31]. Although the excellent efficiency of $CuFe_2O_4$ has been explained by its ability activating PDS and PMS into $HO^{\bullet}$, $SO_4^{\bullet-}$, singlet oxygen ($^1O_2$), there are still some discrepancies in the literature and the current published reports lack a detailed explanation of the differences in the activation mechanisms of the $CuFe_2O_4$/PMS and $CuFe_2O_4$/PDS systems. Furthermore, the differences in the reaction mechanisms in the dark and under UVA light are not been yet thoroughly compared.

In this study, the ability of $CuFe_2O_4$ synthesized in the form of nanopowder was evaluated through the degradation of BPA as model pollutant. The effects of UVA radiation, catalyst and oxidant precursors dosage were investigated on the BPA degradation efficiency. The different activation mechanisms and involvement of reactive species generated from PMS and PDS containing systems were elucidated. Finally, the simultaneous degradation of different phenolic compounds (BPA, phenol and p-nitrophenol) using $CuFe_2O_4$ were investigated in real water matrices to highlight potential applications. The results of this work aimed to demonstrate that SR-AOP containing $CuFe_2O_4$ was a prominent approach for purifying any contaminated water, thus highlighting the potential reuse of the treated waters in the circular economy.

2. Materials and methods

2.1 Chemicals

The details of the chemicals used in this study are listed in Text S1. All chemicals were used as received without purification and unless otherwise specified, Milli-Q water (18 MΩ cm) was used in all experiments.

2.2 Preparation and characterization of $CuFe_2O_4$

$CuFe_2O_4$ nanopowder was synthesized using a single-pot hydrothermal method with polyethylene glycol (PEG) as a structure directing agent. Briefly, a 40 mL solution of 50 mM of $Cu(NO_3)_3 \cdot 3H_2O$ and 100 mM of $Fe(NO_3)_3 \cdot 9H_2O$ was mixed with 1 g of PEG under magnetic stirring. Afterward, the pH was adjusted to 12 using NaOH solution. The solution was then transferred in an autoclave and heated for 24 h at 160 °C. After cooling down, the slurry was centrifuged and the powder was washed with distilled water and ethanol. After drying at 80.0 °C overnight and annealing at 500 °C for 3 h (2.5 °C min^{-1}), $CuFe_2O_4$ nanopowder was obtained.

The crystalline phase composition of the nanopowder was investigated by X-ray diffraction (XRD) using PANalytical X-ray diffractometer (Cu $K\alpha$, λ = 1.5418 Å). The surface morphology was analyzed by scanning electronic microscope coupled to energy dispersive X-ray spectroscopy (SEM/EDX) using Tescan Lyra III instrument. The chemical state of the elements at the surface of the nanopowder was investigated by X-ray photoelectron spectroscopy (XPS) equipped with monochromatic Al $K\alpha$ X-rays (1486.6 eV) and spectra was measured at ambient temperature with photoemission of 45° from the surface. A low energy electron gun (below 1 eV) had been used for charge neutralization to reduce the effects of charging. The XPS analyses was performed before and

after the use of $CuFe_2O_4$ to characterize its surface composition but also to clarify the mechanism of PDS and PMS activation. Also, the valence band maximum (VBM) was also determined using ultraviolet photoelectron spectroscopy (UPS) by a He discharge lamp with a photon energy of 21.22 eV. To investigate the stability of the nanopowder, the concentration of leaching metals including Cu and Fe was determined during the pollutant degradation by atomic absorption spectrophotometry (AAS, PerkinElmer). The samples were first filtered using a PTFE 0.22 µm filter prior for analyses while 10 µM of $Fe(SO_4)$ and $Cu(SO_4)$ solution were prepared and used for the calibration curve. The detection wavelength was set at 248.3 nm and 324.8 nm for iron and copper, respectively.

2.3 Degradation setup

High-performance liquid chromatography (HPLC) equipped with a 250 mm x 4.6 mm Nucleodur 100-5 C18 column was used to quantify the concentrations of BPA, phenol, and p-nitrophenol (Table S1) with the UV detector set at 277 nm, 221 nm, and 315 nm, respectively. The mobile phase was composed of water and acetonitrile 40/60 (v/v) in isocratic mode with a flow rate of 1 mL min^{-1} and column temperature of 40°C. Under these conditions, the retention times of BPA, phenol, and p-nitrophenol were 5.6, 2.7 and 3.1 min. The degradation kinetics were fitted using the pseudo-first-order kinetic model (Eq. 1).

$$ln\frac{C}{C_0} = -k't \qquad \text{(Eq. 1)}$$

where the C represents the residual concentration of the pollutant at t min, and C_0 was for the initial concentration of the pollutant, k' (min^{-1}) is the degradation constant.

During the pollutant degradation, the initial pH was fixed at 6.2, and different experimental parameters including PDS and PMS concentrations (from 0 to 5 mM), catalyst dosage (from 0 to

0.5 g L^{-1}) and light vs. dark conditions were investigated. The activation mechanism of PDS and PMS by $CuFe_2O_4$, quenching experiments were performed during the BPA degradation. Isopropanol (Isop) could simultaneously quench $SO_4^{\bullet-}$ and $HO^{\bullet}$ with a second-order rate constant of 8.2×10^7 M^{-1} s^{-1} and 1.9×10^8 M^{-1} s^{-1}, respectively, while TBA could selectively scavenge $HO^{\bullet}$ with a constant of 6.0×10^8 M^{-1} s^{-1} [32, 33]. It was well known that furfuryl alcohol (FFA) can quench singlet oxygen ($^1O_2$) with a second-order rate constants of 1.2×10^8 M^{-1} s^{-1}) [34], but also can react with $HO^{\bullet}$ and $SO_4^{\bullet-}$ [18]; therefore, $^1O_2$ contribution was evaluated by adding FFA and Isop. Also, PMSO was employed to investigate the potential role of high valent iron that might be present at the surface of the material during degradation reactions. The role of dissolved oxygen was also assessed by comparison with degradation experiments done under N_2 saturated conditions.

To highlight the potential application of $CuFe_2O_4$, real water matrices including tap water (TW) but also sewage treatment plant water (STPW) were used for the degradation of BPA, phenol and p-nitrophenol. The physico-chemical characteristics of TW and STPW matrices were presented in Table S2. Finally, the reusability of $CuFe_2O_4$ in the activation of PDS and PMS was evaluated.

3. Results and discussion

3.1 Material characterization

The crystalline phase composition of the nanopowder had been examined by XRD (Fig. S1). The nanopowder was predominantly composed of $CuFe_2O_4$ (PDF 00-034-0425; space group *I41/amd*) with some impurities identified as CuO and Fe_2O_3 (Fig. S1). These separated impurities were the results of the method of synthesis which cannot avoid their formation from the Cu and Fe precursors, but their presence was assumed to not affect the overall efficiency of $CuFe_2O_4$

nanopowder. Indeed, the $CuFe_2O_4$ diffractions were relatively broads compared to that of the impurities, thus indicating nanosized crystallites with coherent domain size 26 ±13 nm. The SEM pictures of $CuFe_2O_4$ (Fig. 1) showed particle size of about 160 nm. In addition, the particles have a cuboidal morphology which was in accordance with the tetragonal structure (Fig. 1).

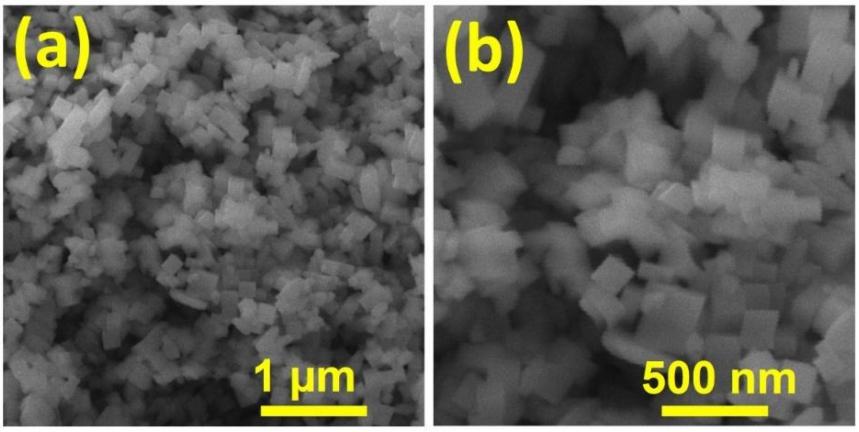

Fig 1. *SEM pictures of $CuFe_2O_4$ nanopowder.*

The chemical composition and oxidation state in $CuFe_2O_4$ nanopowder had been further examined by XPS (Fig. S2). Four main peaks with binding energies of 294, 529, 710 and 933 eV corresponded to the C 1s, O 1s, Fe 2p, and Cu 2p elements, respectively (Fig. S2a). On examining the high resolution XPS spectra, the Cu 2p signal (Fig. S2b) exhibited two symmetric peaks at 933.3 eV and 953.6 eV (along with a satellite peak at 941.4 eV) that corresponded to the binding energies of $2p_{3/2}$ and $2p_{1/2}$ Cu(II), respectively [35]. For the Fe 2p spectrum (Fig. S2c), the asymmetric peak of Fe $2p_{3/2}$ at 710.9 eV can be deconvoluted into two signal that correspond to binding energies of Fe(II) and Fe(III) [36]. Furthermore, the O 1s signal (Fig. S2d) can be deconvoluted into two peaks at 529.4 and 531.5 eV that corresponded to lattice oxygen and surface hydroxyl groups [37, 38], while the C1s signal centered at 294 eV (Fig. S2e) was attributed to

residual carbon from PEG and/or adsorbed organic species from air [39]. The XPS results confirmed the high purity of $CuFe_2O_4$ nanopowder. In addition, the UPS (Fig. S2f) exhibited that the VBM of $CuFe_2O_4$ was located at 4.0 eV, thus $CuFe_2O_4$ was a relatively strong oxidant that might activate PMS and PDS with the photogenerated charge carriers *i.e.*, e^- and h^+.

3.2 Effect of reaction conditions on catalytic degradation of BPA

A first set of experiments using 0.5 g L^{-1} of $CuFe_2O_4$ were provided in the presence of 2 mM of PDS and PMS in the dark and under UVA light to assess the ability of the nanopowder to activate the oxidants. As depicted in Fig. 2a, less than 5% of BPA was degraded after 1h either under UVA light (direct photolysis) or in the presence of $CuFe_2O_4$ (photocatalysis) after 1h. In the presence of 2 mM of PDS and PMS under UVA light (and without $CuFe_2O_4$), the degradation efficiency of BPA slightly increaseed to 13% and 11% after 1hour of reaction. However, the combination of $CuFe_2O_4$ with PDS and PMS resulted in a considerable BPA removal both in the dark and under UVA light. In the dark, the $CuFe_2O_4$/PDS system degraded 45% of BPA within 1 hour, while $CuFe_2O_4$/PMS system exhibited a complete BPA degradation within 20 min. Moreover, higher efficiencies were observed in the presence of UVA where complete BPA degradation was obtained after only 15 min using $CuFe_2O_4$ and PMS, while 72% of degradation was reached within 1 hour in the presence of PDS. To compare the degradation efficiencies of each system, the BPA degradation constants for each system had been reported in Fig. 2b. It was clear that a strong synergistic effect (SE) observed when both catalyst and oxidants occurred either in the dark and UVA light. The SE of the $CuFe_2O_4$/oxidant systems both in the dark and under UVA process can be determined with the following formula:

$$SE(UVA) = \frac{k'_{(UVA+CuFe2O4+oxidant)}}{k'_{(UVA)}+k'_{(oxidant)}+k'_{(CuFe2O4)}} \quad \text{(Eq. 2)}$$

$$SE(Dark) = \frac{k'_{(CuFe2O4+oxidant)}}{k'_{(oxidant)}+k'_{(CuFe2O4)}} \quad \text{(Eq. 3)}$$

where $k'_{(UVA)}$, $k'_{(oxidant)}$, $k'_{(CuFe2O4)}$ and $k'_{(UVA + CuFe2O4 + oxidant)}$ are the BPA degradation constants (min^{-1}) of the mentioned system.

As reported in Fig. 2b, the degradation constants of the multi-factor system ($CuFe_2O_4$/oxidant/dark and UVA) were significantly enhanced compared to the addition of single-factor systems. Indeed, the values of SE calculated for PDS/$CuFe_2O_4$, UVA/PDS/$CuFe_2O_4$, PMS/$CuFe_2O_4$ and UVA/PMS/$CuFe_2O_4$ systems were 3.2, 3.8, 22.4, and 34.1 respectively.

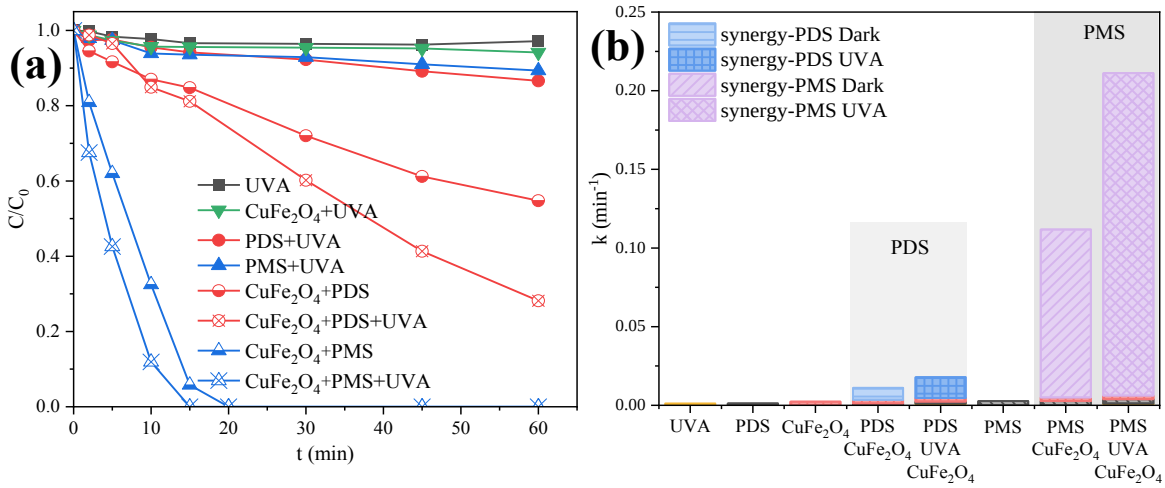

Fig. 2*. a) BPA degradation in different systems, b) BPA degradation constant in PDS and PMS systems under dark and UVA. Initial conditions: [BPA] = 25 μM, pH_0 = 6.2, [PDS] = [PMS] = 2 mM, [$CuFe_2O_4$] = 0.5 g L^{-1}.*

Further experiments had been carried out to explore the effects of $CuFe_2O_4$ and oxidants concentrations on the BPA degradation in the dark and under UVA light (Fig. S3 and S4). When

different $CuFe_2O_4$ dosages (from 0 to 0.5 g L^{-1}) were tested, a similar trend was observed for both PDS and PMS. Under dark and UVA light, the increase of catalyst dosage improved the degradation efficiency of BPA in solution within 60 min (Fig. S2). This result could be ascribed to the increase of exposed active sites that would facilitate the activation of PMS and PDS oxidants. The corresponding BPA degradation constants were reported in Fig. 3a and b. Briefly, when the catalyst dosage was 0.5 g L^{-1}, the degradation constant of BPA in the $CuFe_2O_4$/PMS/UVA system was 0.211 min^{-1} (Fig. 2a), which was about 5.1, 10.0, and 15.1 times that of 0.2 g L^{-1} (0.041 min^{-1}), 0.1 g L^{-1} (0.021 min^{-1}) and 0.05 g L^{-1} (0.014 min^{-1}) of $CuFe_2O_4$ respectively. Similarly, the k' was 0.016 min^{-1} using 0.5 g L^{-1} of catalyst in $CuFe_2O_4$/PDS/UVA system (Fig. 3b), which was about 1.2, 2.7, and 3.2 times the value determined with 0.2 g L^{-1} (0.013 min^{-1}), 0.1 g L^{-1} (0.006 min^{-1}) and 0.05 g L^{-1} (0.005 min^{-1}) respectively.

Experiments using different oxidant concentrations (from 0 to 5 mM) show that in the PMS containing systems (Fig. S4a and b), the degradation efficiency of BPA was significantly enhanced when the PMS concentration increased from 0 to 5 mM, while in the case of PDS containing systems (Fig. S4c and d), the degradation efficiency of BPA increased and then decreased as the PDS concentration increases to 5 mM. The highest degradation constant of BPA reached 0.28 min^{-1} for 5 mM PMS and 0.018 min^{-1} for 2 mM PDS (Fig. 3c and d). The observed decline in the PDS system suggested that the concentration of oxidant precursors was the controlling factor for the $CuFe_2O_4$/PDS systems and that might be due to scavenging effect of PDS toward generated reactive species such as $HO^{\bullet}$ and $SO_4^{\bullet-}$ [40].

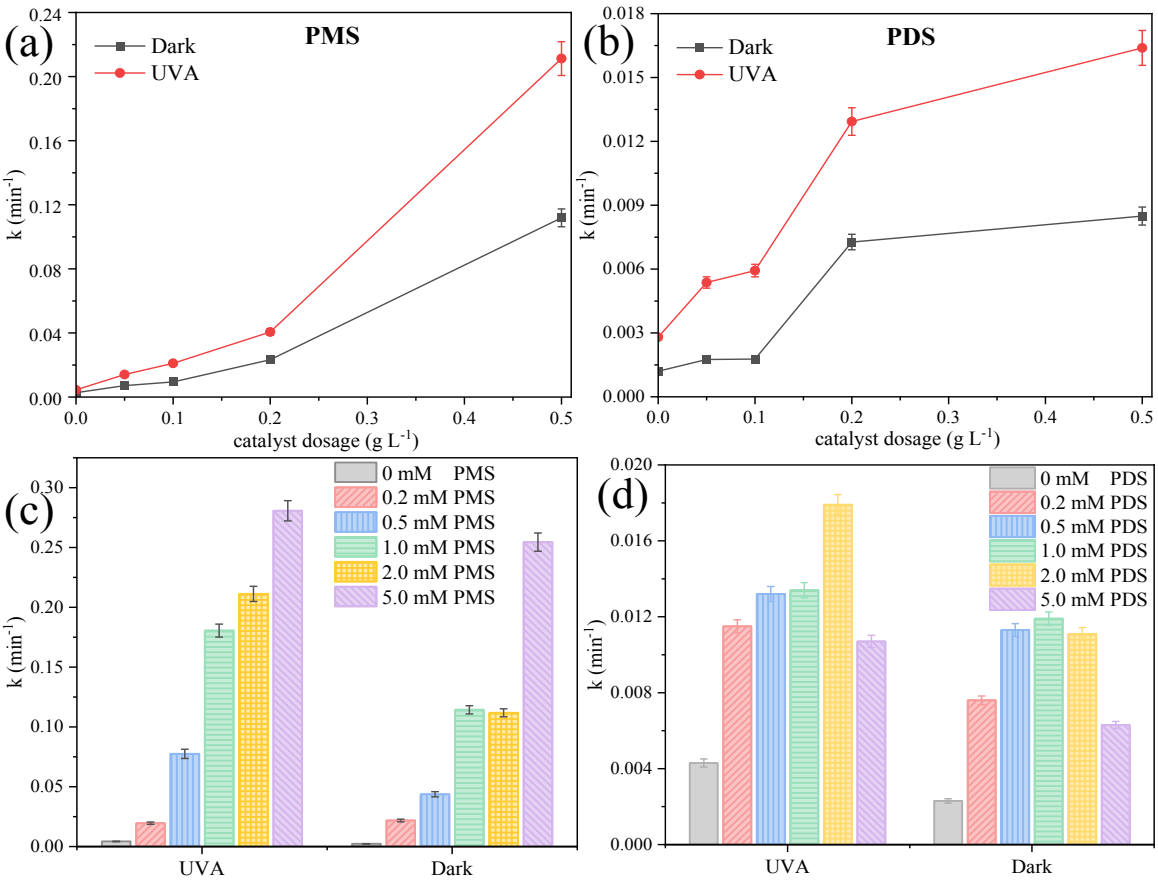

Fig. 3. *Reaction rate constant of the BPA degradation with (a,b) different catalyst dosages in 2mM PMS and PDS and (c,d) different oxidant concentration using 0.5 g* L^{-1} $CuFe_2O_4$*. Initial conditions:* $[BPA] = 25\ \mu M$, $pH_0 = 6.2$.

Based on the above results, 0.5 g L^{-1} of $CuFe_2O_4$ and 2 mM of PMS/PDS were selected as the optimal conditions for further experiments in order to understand the activation mechanism of oxidant using $CuFe_2O_4$. Under adopted experimental conditions, the decrease of the degradation constant of BPA followed the order: $CuFe_2O_4$/PMS/UVA (0.211 min^{-1}) > $CuFe_2O_4$/PMS (0.112 min^{-1}) > $CuFe_2O_4$/PDS/UVA (0.018 min^{-1}) > $CuFe_2O_4$/PDS (0.011 min^{-1}). The degradation efficiency of BPA in the $CuFe_2O_4$/PMS was much higher than value in $CuFe_2O_4$/PDS systems, which may be due to the asymmetric structure of PMS, being easier to activate. The addition of

UVA light significantly increaseed the degradation of BPA in the both systems. Further experiments were carried out to clarify the activation mechanism.

3.3 Oxidant activation mechanism and involvement of reactive species

To gain in-depth mechanistic insights into the oxidant activation in $CuFe_2O_4$/PMS and $CuFe_2O_4$/PDS systems, scavenging experiments had been conducted to identify the generated reactive oxygen species (ROS) both in the dark and under UVA (Fig. 4 and S5).

In the presence of TBA, Isop, or a combination of Isop + FFA, in the $CuFe_2O_4$/PMS system, noticeable reductions in the degradation constants of BPA were observed, with values decreasing from 0.112 to 0.059, 0.045, and 0.018 min^{-1}, respectively (Fig. 4a). In the presence of UVA light, the BPA degradation constants also decreased from 0.211 to 0.159, 0.047, and 0.027 min^{-1} following the introduction of TBA, Isop, Isop + FFA (Fig. 4a). Regarding the contribution of these ROS in the degradation of BPA (Text S2), $HO^{\bullet}$ had a predominant role in the dark (47%) while $SO_4^{\bullet-}$ was identified as the main reactive species under UVA (53%). In addition, the PMS containing systems had been also purged using N_2 to eliminate dissolved O_2. At such conditions, a decrease of BPA degradation rate of 73% in the dark and 66% under UVA was observed, thus indicating that a part of ROS was derived from dissolved O_2 but also from the action of PMS. On the other hand, in the $CuFe_2O_4$/PDS systems (Fig. 4b), the addition of the different scavengers led to a small decrease of the BPA degradation constant highlighting a limited contribution of $HO^{\bullet}$, $SO_4^{\bullet-}$ and $^1O_2$. In addition, the N_2 purging experiments demonstrated a limited effect of oxygen concentration on the degradation of BPA, suggesting the also the presence of non-radical degradation pathway.

The common characteristic of these systems was the BPA degradation enhancement when UVA

light was used. Indeed, UVA can further promote the generation of ROS by the cleavage of the peroxo bond of PMS and PDS (Eqs. 4 and 5) [41], but also can lead to the photolysis of surface Fe(III), thus generating $HO^{\bullet}$ (Eq. 6) [42]. In addition, $CuFe_2O_4$ is a known semiconductor photocatalyst with a highly positive VBM (Figure S2f), thus the photogenerated e^- and h^+ can activate the oxidants (Eqs. 7 and 8) [43].

$$HSO_5^- \xrightarrow{\hbar v} SO_4^{\bullet-} + HO^{\bullet} \quad \text{(Eq. 4)}$$

$$S_2O_8^- \xrightarrow{\hbar v} 2SO_4^{\bullet-} \quad \text{(Eq. 5)}$$

$$\text{Fe(III)} + H_2O \xrightarrow{\hbar v} \equiv \text{Fe(II)} + HO^{\bullet} + H^+ \quad \text{(Eq. 6)}$$

$$CuFe_2O_4(e_{CB}^-) + HSO_5^- \xrightarrow{\hbar v} SO_4^{\bullet-} + HO^- \quad \text{(Eq. 7)}$$

$$CuFe_2O_4(h_{VB}^+) + HSO_5^- \xrightarrow{\hbar v} SO_5^{\bullet-} + H^+ \quad \text{(Eq. 8)}$$

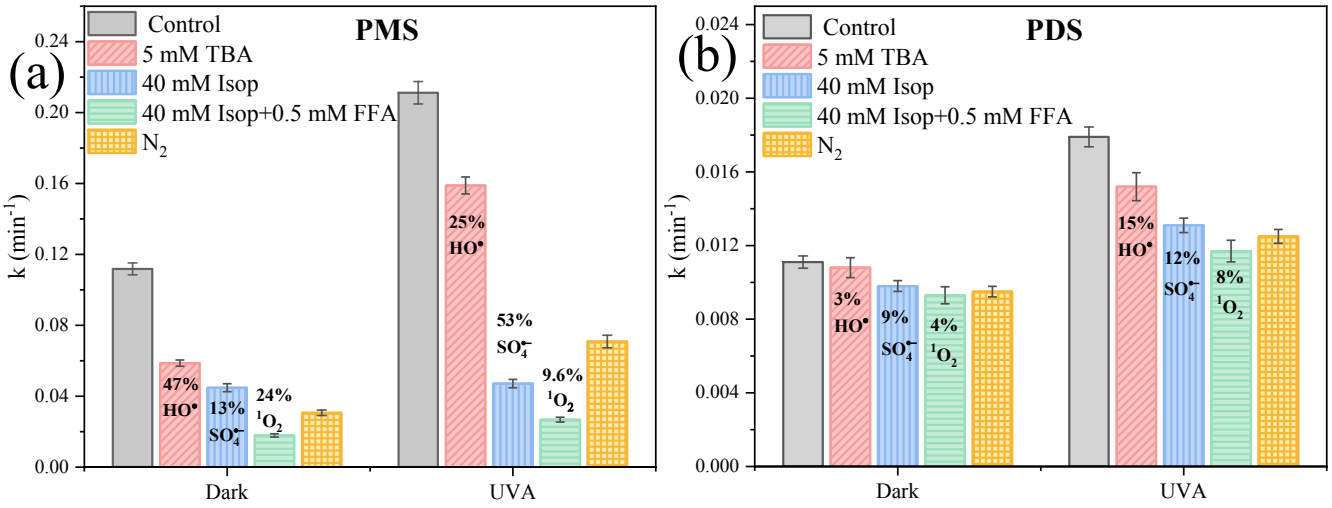

Fig. 4*. The BPA degradation constant (k') of quenching experiments in the various systems. Initial conditions: [BPA] = 25 μM, [$CuFe_2O_4$] = 0.5 g L^{-1}, [TBA] = 5 mM, [Isop] = 40 mM, [FFA] = 0.5 mM, [PS] = [PMS] = 2 mM, pH_0 = 6.2.*

The above data were summarized in Fig. 5. To further clarify the mechanism of oxidant activation,

the generation of high valent iron was first checked since surface Fe(III) might be oxidized into Fe(IV) [18]. Fe(IV) can react with PMSO to produce $PMSO_2$ (Fe(IV): $PMSO_2$=1:1), but in all the investigated systems, no $PMSO_2$ was detected (Fig. S6) which excludes the role of Fe(IV) in the activation of PMS and PDS.

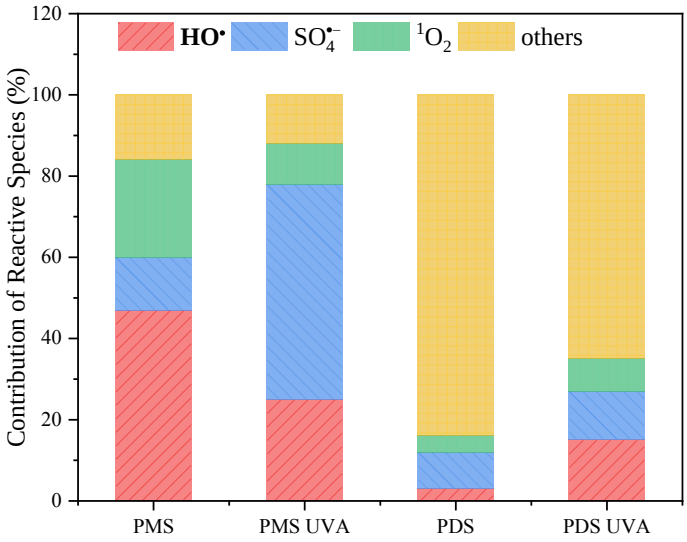

Fig. 5. Contribution of the reactive oxygen species to the BPA degradation over $CuFe_2O_4$ in different systems. Initial conditions: [BPA] = 25 μM, [$CuFe_2O_4$] = 0.5 g L^{-1}, [PS] = [PMS] = 2 mM, pH_0 = 6.2 ± 0.1, 20 ℃.

It might be plausible that the leached metal from $CuFe_2O_4$ i.e., Cu^{2+} and Fe^{3+} can be involved in the activation of PMS and PDS *via* homogeneous reactions. Therefore, the concentrations of Cu^{2+} and Fe^{3+} in the solutions were determined during the BPA degradation using 0.5 g L^{-1} $CuFe_2O_4$ (Fig. S7). No Fe ion leaching from $CuFe_2O_4$ was detected, as the concentrations solution are below the detection limit while the concentration of leached Cu ion in PMS system was about 26.1 mg L^{-1} after 15 min, which was 15.5 times higher than that of the PDS system in 60 min (1.7 mg L^{-1}). However, the contribution of Cu ions to the degradation of BPA was minor, since about 4% and 15%

degradation extent was observed Cu(II)/PMS and Cu(II)/PMS/UVA, respectively (Fig. S8). These results suggested that the degradation of BPA follows a heterogeneous reaction.

The oxidation state modification of $CuFe_2O_4$ in the presence of PMS and PDS was explored using XPS analysis. In fact, the transition metals with higher oxidation state, here Fe^{3+}, can generate peroxymonosulfate or persulfate radicals ($SO_5^{\bullet-}$ and $S_2O_8^{\bullet-}$, Eqs. 9 and 11) and Fe^{2+}. This latter can further decomposed PMS/PDS to generate more powerful reactive radicals ($SO_4^{\bullet-}$, Eqs. 10 and 12). In this way, the redox cycle of Fe(III)/Fe(II) being the limit step [44-46]. The high resolution XPS spectra of Fe (Fig. S9) showed some variation in the ratio Fe^{3+}/Fe^{2+} upon reaction with BPA and/or oxidant.

$$\equiv \mathrm{Fe(III)} + HSO_5^- \rightarrow \equiv \mathrm{Fe(II)} + SO_5^{\bullet-} + H^+ \quad \text{(Eq. 9)}$$

$$\equiv \mathrm{Fe(II)} + HSO_5^- \rightarrow \equiv \mathrm{Fe(III)} + SO_4^{\bullet-} + HO^- \quad \text{(Eq. 10)}$$

$$\equiv \mathrm{Fe(III)} + S_2O_8^- \rightarrow \equiv \mathrm{Fe(II)} + S_2O_8^{\bullet-} \quad \text{(Eq. 11)}$$

$$\equiv \mathrm{Fe(II)} + S_2O_8^- \rightarrow \equiv \mathrm{Fe(III)} + SO_4^{\bullet-} + SO_4^{2-} \quad \text{(Eq. 12)}$$

On the other hand, the transition metals with lower oxidation state *i.e.*, Cu^{2+}, can also be involved during the PMS and PDS activation. Some authors have already suggested the involvement of Cu(III)/Cu(II) redox cycle for the activation of these oxidants [47, 48], but this pathway was excluded in our work since the XPS did not exhibit Cu^{3+} formation during the PMS/PDS activation (Fig. 6). Indeed, Cu(I) was detected by XPS after oxidant activation. After the reaction with PMS, the asymmetric Cu $2p_{3/2}$ signal can be deconvoluted into two peaks with binding energy of 932.7 and 933.8 eV which were associated with the Cu^+ and Cu^{2+} [49], while before reaction, no Cu^+

signal was present (Fig. 6). Based on these results, the suggested activation mechanism of PMS and PDS by Cu^{2+} followed a Cu(II)/Cu(I) redox cycle similar to that of Fe(III)/Fe(II) (Eqs. 13-16) [31, 50]. Furthermore, because of the standard reduction potential of Cu(II)/Cu(I) was lower (0.17 V) than that of Fe(III)/Fe(II) (0.77 V), the reduction of Fe^{3+} by Cu^{+} was thermodynamically feasible (Eq. (17)), which was an advantage in the regeneration of surface Fe(II) [39].

$$\equiv \mathrm{Cu(II)} + HSO_5^- \rightarrow \equiv \mathrm{Cu(I)} + SO_5^{\bullet-} + H^+ \quad \text{(Eq. 13)}$$

$$\equiv \mathrm{Cu(I)} + HSO_5^- \rightarrow \equiv \mathrm{Cu(II)} + SO_4^{\bullet-} + HO^- \quad \text{(Eq. 14)}$$

$$\equiv \mathrm{Cu(II)} + S_2O_8^- \rightarrow \equiv \mathrm{Cu(III)} + SO_4^{\bullet-} + SO_4^{2-} \quad \text{(Eq. 15)}$$

$$\equiv \mathrm{Cu(I)} + S_2O_8^- \rightarrow \equiv \mathrm{Cu(II)} + SO_4^{\bullet-} + SO_4^{2-} \quad \text{(Eq. 16)}$$

$$\equiv \mathrm{Cu(I)} + \equiv \mathrm{Fe(III)} \rightarrow \equiv \mathrm{Cu(II)} + \equiv \mathrm{Fe(II)} \quad \text{(Eq. 17)}$$

However, this mechanism did not play a major role in the case of the PDS activation by $CuFe_2O_4$ either in the dark or under UVA (Fig. 5). Therefore, a non-radical mechanism was assumed and the XPS data confirm this pathway (Fig. 6). In fact, after reaction with PDS, the Cu $2p_{3/2}$ signal remained symmetric, thus no changes were observed (Fig. 6). With the addition of BPA, the signal became asymmetric due to the presence of Cu^{+} (Fig. 6), thus suggesting an electron transfer from BPA to PDS *via* $CuFe_2O_4$ as electron mediator [51, 52].

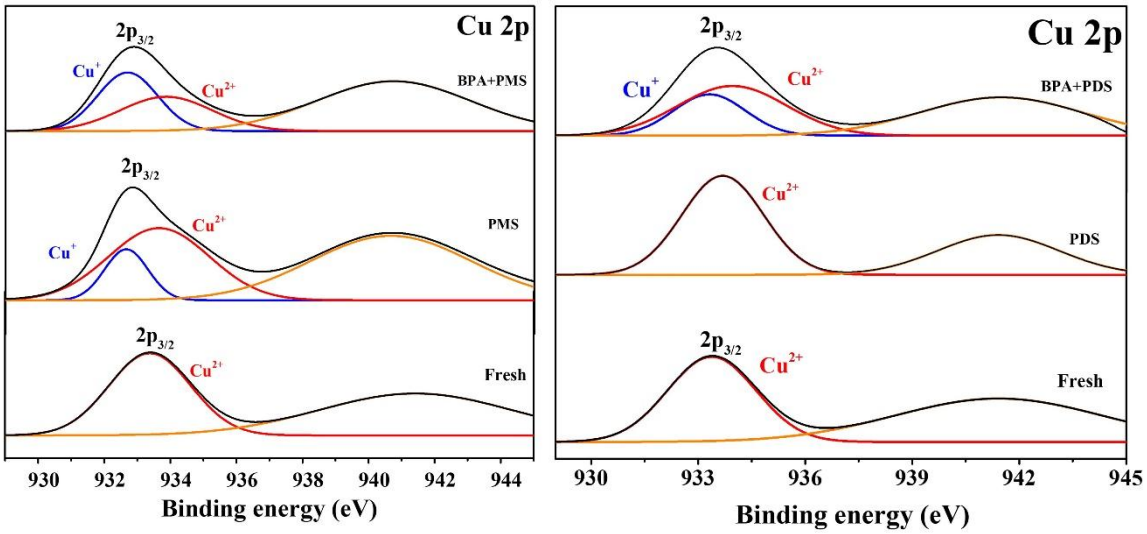

Fig. 6. *High-resolution XPS spectra of Cu $2p_{3/2}$ signal for freshly prepared $CuFe_2O_4$, $CuFe_2O_4$ in PMS/PDS solution and $CuFe_2O_4$ in PMS/PDS + BPA solution.*

In addition, the O 1s signal of $CuFe_2O_4$ can be deconvoluted into lattice (bulk O^{2-}) and surface oxygen *i.e.*, surface hydroxyl group (Fig. S10). In both PMS and PDS containing systems, the number of surface hydroxyl groups increaseed during activation of the oxidants, thus suggesting an important role of this functional groups in both radical and non-radical mechanism.

3.4 Reusability of $CuFe_2O_4$ and its application in different water matrices

In order to assess the reusability of $CuFe_2O_4$, the degradation of BPA was tested during recycling experiments. As shown in Fig. 7, the $CuFe_2O_4$/PMS/UVA system demonstrated a higher degradation efficiency than the PDS containing system at the first use.

However, the BPA degradation in the PMS containing system significantly decreaseed from 100% to 32% in the second cycle with the reuse of $CuFe_2O_4$ (Fig. 7a). On the contrary, $CuFe_2O_4$ was much more stable for activating PDS (Fig. 7b), since a slower decrease was observed with BPA

degradation efficiency degrading from 72%, to 29% after three cycles. The observed decrease can be due to the leaching of copper which was more significant in the PMS containing system, thus explaining the differences between PMS and PDS containing systems. Also, the XPS analyses showed significant changes at the surface of the $CuFe_2O_4$ after its use for PMS and PDS activation, and that might also a reason to explain its low reusability.

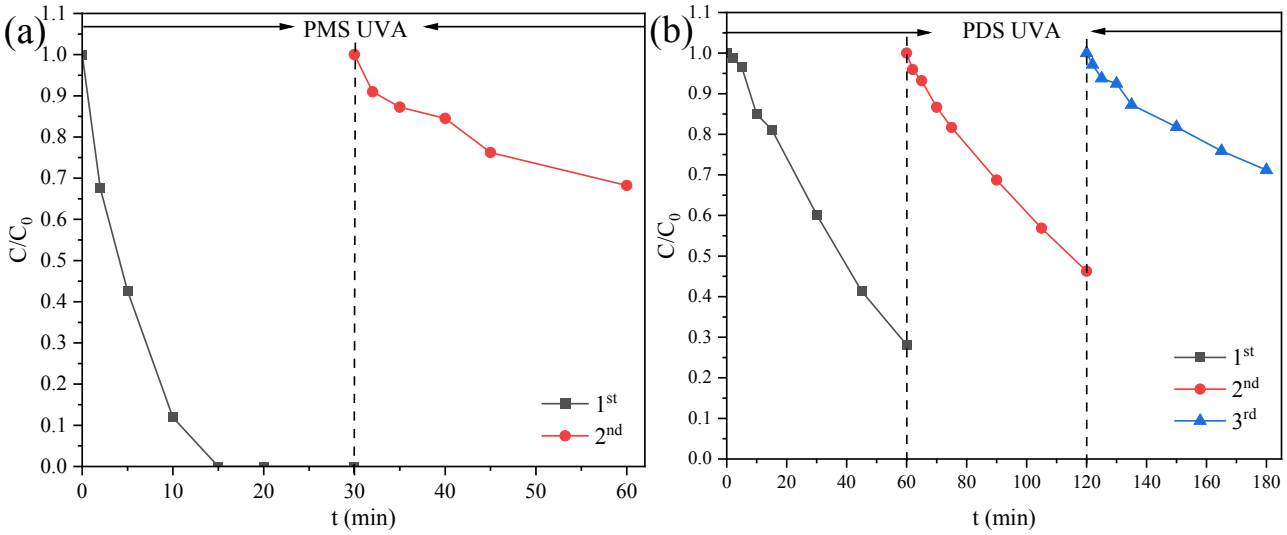

Fig. 7. *The reusability of $CuFe_2O_4$ for BPA degradation in PMS system (a) and PDS system (b). Initial conditions: [$CuFe_2O_4$] = 0.5 g L^{-1}, [PMS] = [PDS] = 2 mM, pH_0 = 6.2.*

The degradation efficiency of $CuFe_2O_4$ in pure water, TW and STPW was investigated for three phenolic organic pollutants (BPA, phenol and p-nitrophenol) (Fig. 8). In pure water system (Fig. 8a), all target pollutants can be completely degraded within 20 min in $CuFe_2O_4$/PMS/UVA. As expected, the degradation rate of all three pollutants decreased significantly in both the tap water (Fig. 8c) and STPW (Fig. 8e). This effect was due to presence of inorganic anions and natural organic matter, which can partially quench the generated ROS. However, in STPW (Fig. 8e), phenol and p-nitrophenol were degraded up to 90% and 61%, which were good degradation extents after only

30 min in $CuFe_2O_4$/PMS/UVA system. The degradation efficiencies for the three pollutants in this system followed the order BPA > phenol > p-nitrophenol, which was the same observed trend as in the case of the PDS system. In this latter system, although the degradation of BPA remained relatively efficient in pure water (100%), TW (75%) and STPW (64%), the degradation rate of phenol and p-nitrophenol significantly decreases in TW and STPW (Fig. 8b, d and f).

The degradation efficiencies observed for the three phenolic compounds can be correlated with their O–H bond dissociation energies (BDE) where the values have been already reported by H. Su et al. [53] (Table S1). In addition, for phenolic organic contaminants, the BDE of C–H bond is higher than that of O-H bond, thus the compounds with electron donating groups (such as OH) are more reactive. Therefore, BPA which had a smaller BDE and more electron-donating groups compared to phenol and p-nitrophenol was easier to degrade.

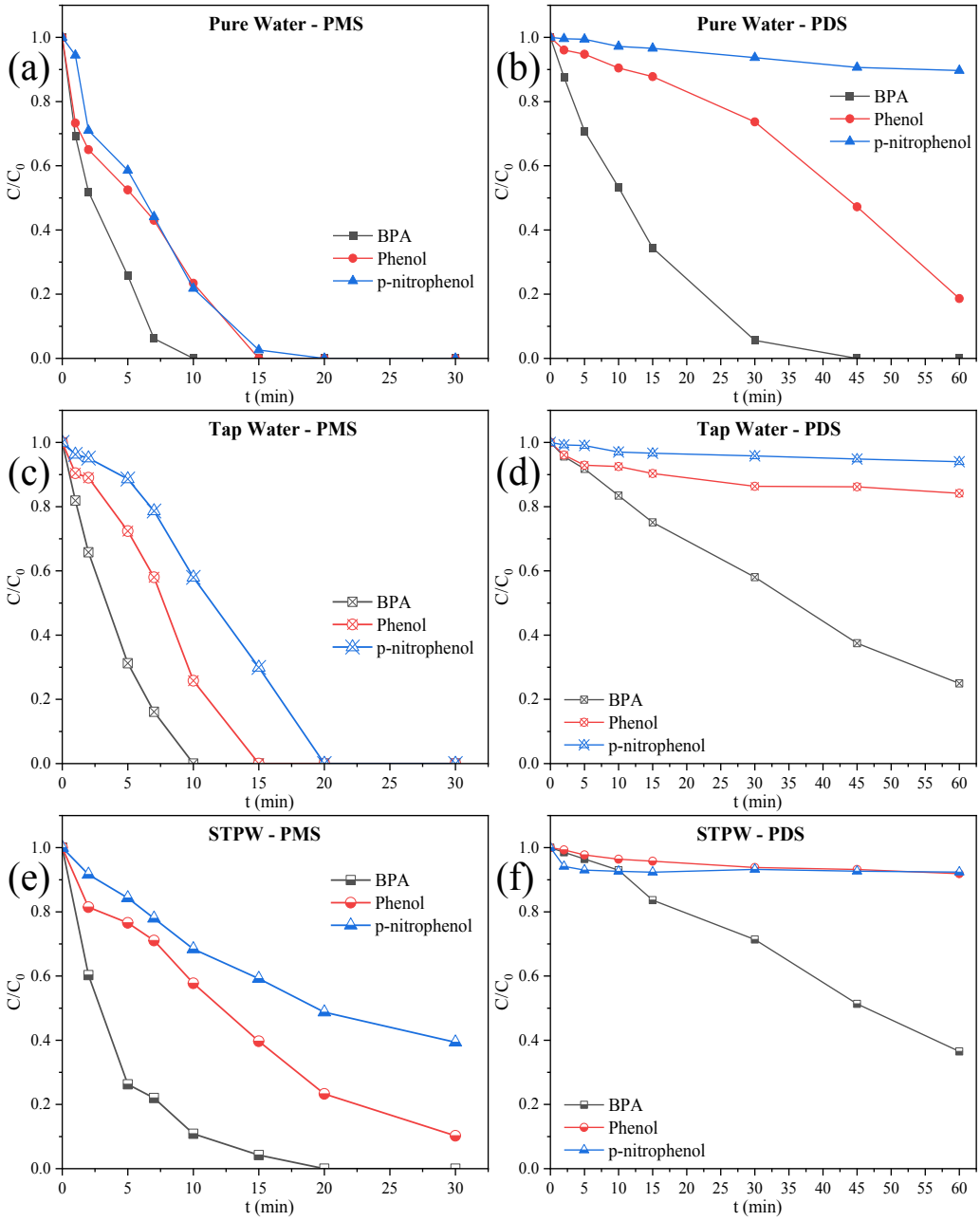

Fig. 8. *The degradation efficiency of mixed solution by $CuFe_2O_4$ under UVA in virous water matrix: (a) PMS in pure water, (b) PDS in pure water, (c) PMS in tap water, (d) PDS in tap water, (e) PMS in STPW, and (f) PDS in STPW. Initial conditions: [$CuFe_2O_4$] = 0.5 g L^{-1}, [PMS] = [PDS] = 2 mM, [BPA] = [Phenol] = [p-nitrophenol] = 5 μM, pH_0 = 6.2.*

4 Conclusion

In this study, the mechanism of PMS and PDS activation using $CuFe_2O_4$ both in the dark and under UVA was clarified while the effect of different experimental parameters was also investigated for the BPA degradation to determine optimal conditions. In brief, the selected conditions were 0.5 g L^{-1} of $CuFe_2O_4$ and 2 mM of PMS/PDS under pH_0 = 6.2 $\pm$ 0.1. For the degradation of BPA, $CuFe_2O_4$ coupling with PMS demonstrated better degradation than PDS-containing systems. The reaction rate constants of BPA degradation followed the order: $CuFe_2O_4$/PMS/UVA (0.211 min^{-1}) > $CuFe_2O_4$/PMS (0.112 min^{-1}) > $CuFe_2O_4$/PDS/UVA (0.018 min^{-1}) > $CuFe_2O_4$/PDS (0.011 min^{-1}). Radical quenching experiments suggested that the BPA degradation followed a radical pathway in PMS-containing systems with $SO_4^{\bullet-}$ as the main reactive species while for PDS-containing systems, a non-radical pathway was predominant. Indeed, XPS analyses exhibited that surface copper played an important role and electron transfer from the pollutant to the catalyst and then to PDS was suggested. The stability of $CuFe_2O_4$ exhibited leaching of Cu^{2+} (26.1 mg L^{-1} under PMS system and 1.7 mg L^{-1} under PDS system), thus highlighting that this catalyst cannot be reused, especially for PMS activation. However, regarding the complexity of tap and sewage treatment plant waters, the activation of PMS and PDS by $CuFe_2O_4$ catalyst exhibited excellent performance, thus being a promising strategy to develop for wastewaters treatment and their potential reuse in the circular economy of water.

Acknowledgement

This work was partially supported by the Slovak Research and Development Agency (SRDA) under the contract No. APVV-21-0039 and the Scientific Grant Agency of the Ministry of Education, Science, Research and Sport of the Slovak republic (VEGA project No. 1/0319/23), and the Grant

of Comenius University Bratislava for Young Scientists No. UK/226/2023. The presented results are obtained in the frame of the French-Slovak bilateral project “SOLAREM” co-financed by PHC Stefanik program (Campus France) and SRDA under the contract No. SK-FR-22-0002. Finally, authors thank the financial support under the Operational Program Integrated Infrastructure for the projects “Advancing University Capacity and Competence in Research, Development and Innovation” (ACCORD, ITMS2014+:313021X329) and “UpScale of Comenius University Capacities and Competence in Research, Development and Innovation” (USCCCORD, ITMS 2014+: 313021BUZ3), co-financed by the European Regional Development Fund. Authors also acknowledge the Ministry of Education of China for providing the financial support for Minjuan CAI stay in France, the IRP CNRS "Processes for Environmental Remediation" and from the LIA by the project I-site CAP 20-25 and PRC program CNRS/NSFC n°270437

References

[1] Zhu, Z., F. Liu, H. Zhang, J. Zhang, and L. Han, Photocatalytic degradation of 4-chlorophenol over Ag/MFe_2O_4 (M = Co, Zn, Cu, and Ni) prepared by a modified chemical co-precipitation method: a comparative study. RSC Advances. 5 (2015) 55499-55512, 10.1039/C5RA04608D.

[2] Chen, Z., L. Wang, H. Xu, and Q. Wen, Efficient heterogeneous activation of peroxymonosulfate by modified $CuFe_2O_4$ for degradation of tetrabromobisphenol A. Chemical Engineering Journal. 389 (2020) 124345, https://doi.org/10.1016/j.cej.2020.124345.

[3] Mustieles, V., S.C. D'Cruz, S. Couderq, A. Rodríguez-Carrillo, J.-B. Fini, T. Hofer, I.-L. Steffensen, H. Dirven, R. Barouki, N. Olea, M.F. Fernández, and A. David, Bisphenol A and its analogues: A comprehensive review to identify and prioritize effect biomarkers for human biomonitoring. Environment International. 144 (2020) 105811, https://doi.org/10.1016/j.envint.2020.105811.

[4] Panigrahy, N., A. Priyadarshini, M.M. Sahoo, A.K. Verma, A. Daverey, and N.K. Sahoo, A comprehensive review on eco-toxicity and biodegradation of phenolics: Recent progress and future outlook. Environmental Technology & Innovation. 27 (2022) 102423, https://doi.org/10.1016/j.eti.2022.102423.

[5] Balakrishnan, A., G.J. Gaware, and M. Chinthala, Heterojunction photocatalysts for the removal of nitrophenol: A systematic review. Chemosphere. 310 (2023) 136853, https://doi.org/10.1016/j.chemosphere.2022.136853.

[6] Othman, I., M. Abu Haija, I. Ismail, J.H. Zain, and F. Banat, Preparation and catalytic performance of $CuFe_2O_4$ nanoparticles supported on reduced graphene oxide ($CuFe_2O_4$/rGO) for phenol degradation. Materials Chemistry and Physics. 238 (2019) 121931, https://doi.org/10.1016/j.matchemphys.2019.121931.

[7] Abbaszadeh, S., S.R. Wan Alwi, C. Webb, N. Ghasemi, and I.I. Muhamad, Treatment of lead-contaminated water using activated carbon adsorbent from locally available papaya peel biowaste. Journal of Cleaner Production. 118 (2016) 210-222, https://doi.org/10.1016/j.jclepro.2016.01.054.

[8] Gadekar, M.R. and M.M. Ahammed, Coagulation/flocculation process for dye removal using water treatment residuals: modelling through artificial neural networks. Desalination and Water Treatment. 57 (2016) 26392-26400, 10.1080/19443994.2016.1165150.

[9] Pal, S., F. Banat, A. Almansoori, and M. Abu Haija, Review of technologies for biotreatment of refinery wastewaters: progress, challenges and future opportunities. Environmental Technology Reviews. 5 (2016) 12-38, 10.1080/21622515.2016.1164252.

[10] Erkanlı, M., L. Yilmaz, P.Z. Çulfaz-Emecen, and U. Yetis, Brackish water recovery from reactive dyeing wastewater via ultrafiltration. Journal of Cleaner Production. 165 (2017) 1204-1214, https://doi.org/10.1016/j.jclepro.2017.07.195.

[11] Hu, P. and M. Long, Cobalt-catalyzed sulfate radical-based advanced oxidation: A review on heterogeneous catalysts and applications. Applied Catalysis B: Environmental. 181 (2016) 103-117, https://doi.org/10.1016/j.apcatb.2015.07.024.

[12] Ling, L., D. Zhang, C. Fan, and C. Shang, A Fe(II)/citrate/UV/PMS process for carbamazepine degradation at a very low Fe(II)/PMS ratio and neutral pH: The mechanisms. Water Research. 124 (2017) 446-453, https://doi.org/10.1016/j.watres.2017.07.066.

[13] Rao, Y.F., L. Qu, H. Yang, and W. Chu, Degradation of carbamazepine by Fe(II)-activated persulfate process. Journal of Hazardous Materials. 268 (2014) 23-32, https://doi.org/10.1016/j.jhazmat.2014.01.010.

[14] Neta, P., V. Madhavan, H. Zemel, and R.W. Fessenden, Rate constants and mechanism of reaction of sulfate radical anion with aromatic compounds. Journal of the American Chemical Society. 99 (1977) 163-164, 10.1021/ja00443a030.

[15] Antoniou, M.G., A.A. de la Cruz, and D.D. Dionysiou, Degradation of microcystin-LR using sulfate radicals

generated through photolysis, thermolysis and e^- transfer mechanisms. Applied Catalysis B: Environmental. 96 (2010) 290-298, https://doi.org/10.1016/j.apcatb.2010.02.013.

[16] Ding, Y., L. Zhu, N. Wang, and H. Tang, Sulfate radicals induced degradation of tetrabromobisphenol A with nanoscaled magnetic CuFe2O4 as a heterogeneous catalyst of peroxymonosulfate. Applied Catalysis B: Environmental. 129 (2013) 153-162, https://doi.org/10.1016/j.apcatb.2012.09.015.

[17] Lei, X., M. You, F. Pan, M. Liu, P. Yang, D. Xia, Q. Li, Y. Wang, and J. Fu, $CuFe_2O_4$@GO nanocomposite as an effective and recoverable catalyst of peroxymonosulfate activation for degradation of aqueous dye pollutants. Chinese Chemical Letters. 30 (2019) 2216-2220, https://doi.org/10.1016/j.cclet.2019.05.039.

[18] Cai, M., P. Cheng, J. Li, F. Wu, M. Sarakha, G. Mailhot, and M. Brigante, Toward a better understanding of peroxymonosulfate and peroxydisulfate activation using a nano zero-valent iron catalyst supported on graphitized carbon: Mechanisms and application to the degradation of estrogenic compounds in different water matrix. Journal of Cleaner Production. 414 (2023) 137702, https://doi.org/10.1016/j.jclepro.2023.137702.

[19] Jia, D., O. Monfort, K. Hanna, G. Mailhot, and M. Brigante, Caffeine degradation using peroxydisulfate and peroxymonosulfate in the presence of Mn_2O_3. Efficiency, reactive species formation and application in sewage treatment plant water. Journal of Cleaner Production. 328 (2021) 129652, https://doi.org/10.1016/j.jclepro.2021.129652.

[20] Feng, Y., D. Wu, Y. Deng, T. Zhang, and K. Shih, Sulfate Radical-Mediated Degradation of Sulfadiazine by $CuFeO_2$ Rhombohedral Crystal-Catalyzed Peroxymonosulfate: Synergistic Effects and Mechanisms. Environmental Science & Technology. 50 (2016) 3119-3127, 10.1021/acs.est.5b05974.

[21] Ding, Y., X. Wang, L. Fu, X. Peng, C. Pan, Q. Mao, C. Wang, and J. Yan, Nonradicals induced degradation of organic pollutants by peroxydisulfate (PDS) and peroxymonosulfate (PMS): Recent advances and perspective. Science of The Total Environment. 765 (2021) 142794, https://doi.org/10.1016/j.scitotenv.2020.142794.

[22] Wang, Z., W. Qiu, S.-y. Pang, Y. Zhou, Y. Gao, C. Guan, and J. Jiang, Further understanding the involvement of Fe(IV) in peroxydisulfate and peroxymonosulfate activation by Fe(II) for oxidative water treatment. Chemical Engineering Journal. 371 (2019) 842-847, https://doi.org/10.1016/j.cej.2019.04.101.

[23] Xu, Y., J. Ai, and H. Zhang, The mechanism of degradation of bisphenol A using the magnetically separable $CuFe_2O_4$/peroxymonosulfate heterogeneous oxidation process. Journal of Hazardous Materials. 309 (2016) 87-96, https://doi.org/10.1016/j.jhazmat.2016.01.023.

[24] Guan, Y.-H., J. Ma, Y.-M. Ren, Y.-L. Liu, J.-Y. Xiao, L.-q. Lin, and C. Zhang, Efficient degradation of atrazine by magnetic porous copper ferrite catalyzed peroxymonosulfate oxidation via the formation of hydroxyl and sulfate radicals. Water Research. 47 (2013) 5431-5438, https://doi.org/10.1016/j.watres.2013.06.023.

[25] Fröhlich, A.C., E.L. Foletto, and G.L. Dotto, Preparation and characterization of $NiFe_2O_4$/activated carbon composite as potential magnetic adsorbent for removal of ibuprofen and ketoprofen pharmaceuticals from aqueous solutions. Journal of Cleaner Production. 229 (2019) 828-837, https://doi.org/10.1016/j.jclepro.2019.05.037.

[26] Ai, L., H. Huang, Z. Chen, X. Wei, and J. Jiang, Activated carbon/$CoFe_2O_4$ composites: Facile synthesis, magnetic performance and their potential application for the removal of malachite green from water. Chemical Engineering Journal. 156 (2010) 243-249, https://doi.org/10.1016/j.cej.2009.08.028.

[27] Shao, L., Z. Ren, G. Zhang, and L. Chen, Facile synthesis, characterization of a $MnFe_2O_4$/activated carbon magnetic composite and its effectiveness in tetracycline removal. Materials Chemistry and Physics. 135 (2012) 16-24, https://doi.org/10.1016/j.matchemphys.2012.03.035.

[28] Ren, Y., L. Lin, J. Ma, J. Yang, J. Feng, and Z. Fan, Sulfate radicals induced from peroxymonosulfate by magnetic ferrospinel MFe_2O_4 (M=Co, Cu, Mn, and Zn) as heterogeneous catalysts in the water. Applied Catalysis B: Environmental. 165 (2015) 572-578, https://doi.org/10.1016/j.apcatb.2014.10.051.

[29] Feng, Y., C. Liao, and K. Shih, Copper-promoted circumneutral activation of H_2O_2 by magnetic $CuFe_2O_4$ spinel

nanoparticles: Mechanism, stoichiometric efficiency, and pathway of degrading sulfanilamide. Chemosphere. 154 (2016) 573-582, https://doi.org/10.1016/j.chemosphere.2016.04.019.

[30] Wang, Y., H. Zhao, M. Li, J. Fan, and G. Zhao, Magnetic ordered mesoporous copper ferrite as a heterogeneous Fenton catalyst for the degradation of imidacloprid. Applied Catalysis B: Environmental. 147 (2014) 534-545, https://doi.org/10.1016/j.apcatb.2013.09.017.

[31] Zhang, C., Z. Wang, F. Li, J. Wang, N. Xu, Y. Jia, S. Gao, T. Tian, and W. Shen, Degradation of tetracycline by activated peroxodisulfate using $CuFe_2O_4$-loaded biochar. Journal of Molecular Liquids. 368 (2022) 120622, https://doi.org/10.1016/j.molliq.2022.120622.

[32] Buxton, G.V., C.L. Greenstock, W.P. Helman, and A.B. Ross, Critical Review of rate constants for reactions of hydrated electrons, hydrogen atoms and hydroxyl radicals ($\cdot OH/\cdot O^-$ in Aqueous Solution. Journal of Physical and Chemical Reference Data. 17 (1988) 513-886, 10.1063/1.555805.

[33] Huie, R.E., C.L. Clifton, and P. Neta, Electron transfer reaction rates and equilibria of the carbonate and sulfate radical anions. International Journal of Radiation Applications and Instrumentation. Part C. Radiation Physics and Chemistry. 38 (1991) 477-481, https://doi.org/10.1016/1359-0197(91)90065-A.

[34] Mi, X., P. Wang, S. Xu, L. Su, H. Zhong, H. Wang, Y. Li, and S. Zhan, Almost 100 % Peroxymonosulfate Conversion to Singlet Oxygen on Single- Atom CoN 2+2 Sites. Angewandte Chemie. 133 (2021) 4638-4643, 10.1002/ange.202014472.

[35] Dong, X., B. Ren, Z. Sun, C. Li, X. Zhang, M. Kong, S. Zheng, and D.D. Dionysiou, Monodispersed $CuFe_2O_4$ nanoparticles anchored on natural kaolinite as highly efficient peroxymonosulfate catalyst for bisphenol A degradation. Applied Catalysis B: Environmental. 253 (2019) 206-217, https://doi.org/10.1016/j.apcatb.2019.04.052.

[36] Huang, Y., C. Han, Y. Liu, M.N. Nadagouda, L. Machala, K.E. O'Shea, V.K. Sharma, and D.D. Dionysiou, Degradation of atrazine by $ZnxCu_1{-}xFe_2O_4$ nanomaterial-catalyzed sulfite under UV–vis light irradiation: Green strategy to generate SO_4^-. Applied Catalysis B-environmental. 221 (2018) 380-392.

[37] Amini, S., M. Amiri, H. Ebrahimzadeh, S. Seidi, and S. Hejabri kandeh, Synthesis of magnetic $Cu/CuFe_2O_4$@MIL-88A(Fe) nanocomposite and application to dispersive solid-phase extraction of chlorpyrifos and phosalone in water and food samples. Journal of Food Composition and Analysis. 104 (2021) 104128, https://doi.org/10.1016/j.jfca.2021.104128.

[38] Hu, X., B. Liu, Y. Deng, H. Chen, S. Luo, C. Sun, P. Yang, and S. Yang, Adsorption and heterogeneous Fenton degradation of 17α-methyltestosterone on nano Fe_3O_4/MWCNTs in aqueous solution. Applied Catalysis B: Environmental. 107 (2011) 274-283, https://doi.org/10.1016/j.apcatb.2011.07.025.

[39] Zhang, X., Y. Ding, H. Tang, X. Han, L. Zhu, and N. Wang, Degradation of bisphenol A by hydrogen peroxide activated with $CuFeO_2$ microparticles as a heterogeneous Fenton-like catalyst: Efficiency, stability and mechanism. Chemical Engineering Journal. 236 (2014) 251-262, https://doi.org/10.1016/j.cej.2013.09.051.

[40] Ushani, U., X. Lu, J. Wang, Z. Zhang, J. Dai, Y. Tan, S. Wang, W. Li, C. Niu, T. Cai, N. Wang, and G. Zhen, Sulfate radicals-based advanced oxidation technology in various environmental remediation: A state-of-the–art review. Chemical Engineering Journal. 402 (2020) 126232, https://doi.org/10.1016/j.cej.2020.126232.

[41] Rodríguez-Chueca, J., E. Barahona-García, V. Blanco-Gutiérrez, L. Isidoro-García, and A.J. Dos santos-García, Magnetic $CoFe_2O_4$ ferrite for peroxymonosulfate activation for disinfection of wastewater. Chemical Engineering Journal. 398 (2020) 125606, https://doi.org/10.1016/j.cej.2020.125606.

[42] Kattel, E., M. Trapido, and N. Dulova, Oxidative degradation of emerging micropollutant acesulfame in aqueous matrices by UVA-induced H_2O_2/Fe^{2+} and $S_2O_8^{2-}/Fe^{2+}$ processes. Chemosphere. 171 (2017) 528-536, https://doi.org/10.1016/j.chemosphere.2016.12.104.

[43] Xin, J., Y. Liu, L. Niu, F. Zhang, X. Li, C. Shao, X. Li, and Y. Liu, Three-dimensional porous $CuFe_2O_4$ for visible-light-driven peroxymonosulfate activation with superior performance for the degradation of tetracycline hydrochloride. Chemical Engineering Journal. 445 (2022) 136616, https://doi.org/10.1016/j.cej.2022.136616.

[44] Das, T.N.J.T.J.o.P.C.A., Reactivity and role of $SO_5^{\bullet-}$radical in aqueous medium chain oxidation of sulfite to sulfate and atmospheric sulfuric acid generation. 105 (2001) 9142-9155.

[45] Das, T.N., R.E. Huie, and P.J.T.J.o.P.C.A. Neta, Reduction potentials of SO_3•-, SO_5•-, and $S_4O_6^{\bullet 3-}$radicals in aqueous solution. 103 (1999) 3581-3588.

[46] Gholami, P., L. Dinpazhoh, A. Khataee, A. Hassani, and A. Bhatnagar, Facile hydrothermal synthesis of novel Fe-Cu layered double hydroxide/biochar nanocomposite with enhanced sonocatalytic activity for degradation of cefazolin sodium. Journal of Hazardous Materials. 381 (2020) 120742, https://doi.org/10.1016/j.jhazmat.2019.120742.

[47] Zhang, T., H. Zhu, and J.-P. Croué, Production of Sulfate Radical from Peroxymonosulfate Induced by a Magnetically Separable CuFe2O4 Spinel in Water: Efficiency, Stability, and Mechanism. Environmental Science & Technology. 47 (2013) 2784-2791, 10.1021/es304721g.

[48] Li, H., N. Yuan, C. Wang, X. Yan, and J. Qian, New insights into the $CuFe_2O_4$/PMS process: The roles of surface Cu(III) species and free radicals. Chemical Engineering Journal Advances. 15 (2023) 100506, https://doi.org/10.1016/j.ceja.2023.100506.

[49] Lei, Y., C.-S. Chen, Y.-J. Tu, Y.-H. Huang, and H. Zhang, Heterogeneous Degradation of Organic Pollutants by Persulfate Activated by CuO-Fe_3O_4: Mechanism, Stability, and Effects of pH and Bicarbonate Ions. Environmental Science & Technology. 49 (2015) 6838-6845, 10.1021/acs.est.5b00623.

[50] Wang, B., Q. Li, Y. Lv, H. Fu, D. Liu, Y. Feng, H. Xie, and H. Qu, Insights into the mechanism of peroxydisulfate activated by magnetic spinel $CuFe_2O_4$/SBC as a heterogeneous catalyst for bisphenol S degradation. Chemical Engineering Journal. 416 (2021) 129162, https://doi.org/10.1016/j.cej.2021.129162.

[51] Jawad, A., K. Zhan, H. Wang, A. Shahzad, Z. Zeng, J. Wang, X. Zhou, H. Ullah, Z. Chen, and Z. Chen, Tuning of Persulfate Activation from a Free Radical to a Nonradical Pathway through the Incorporation of Non-Redox Magnesium Oxide. Environmental Science & Technology. 54 (2020) 2476-2488, 10.1021/acs.est.9b04696.

[52] Tian, K., F. Shi, M. Cao, Q. Zheng, and G. Zhang *A Review of Persulfate Activation by Magnetic Catalysts to Degrade Organic Contaminants: Mechanisms and Applications*. Catalysts, 2022. **12**, DOI: 10.3390/catal12091058.

[53] Su, H., Y. Wei, X. Qu, C. Yu, Q. Li, P.J.J. Alvarez, and M. Long, Mechanistic inference on the reaction kinetics of phenols and anilines in carbon nanotubes-activated peroxydisulfate systems: pp-LFERs and QSARs analyses. Chemical Engineering Journal. 385 (2020) 123923, https://doi.org/10.1016/j.cej.2019.123923.